A mechanical model for fatigue crack propagation

H. W. LIU and NOBU IINO
Syracuse University, Syracuse, N.Y.

Summary
A mechanical model of fatigue crack propagation is proposed. It hypothesizes that damage due to strain cycling of the material at a crack tip causes propagation. Manson-Coffin's strain cycle fatigue law was used as failure criterion and Miner's law was used for damage accumulation. The proposed theory correlates surprisingly well with data for 2024-T351 Al and 4340 fully annealed steel.

Strains at a crack tip were measured by the moire optical interference method. The strain at a crack tip was proportional to ΔK^2. The results of strain measurements were used to calculate crack propagation rate.

Introduction

In recent years, fatigue crack propagation has been investigated extensively from crack length measurements on the specimen surface [1-14] and from striation studies on fracture surfaces [14-17]. Paris, Gomez and Anderson [4] have proposed a correlation of crack propagation rate with stress intensity factor. Emphasizing the damage caused by cumulative cyclic strains at a crack tip, Liu [5, 8] derived a crack propagation rate for a centrally cracked plate, which is proportional to the plastic zone size, r_p, and $(\Delta\bar{\sigma}^2 a)$ where $\Delta\bar{\sigma}$ is the applied stress range, and 'a' the half crack length. The quantity $(\Delta\bar{\sigma}^2 a)$ is the square of stress intensity factor range, ΔK^2, for a cracked infinite plate.

Paris and Erdogan [6] found from experimental data that propagation rate is proportional to ΔK^4 for a number of materials. The fourth power relation was justified by the consideration of the energy absorption within the entire plastic zone [9]. Ever since, the fourth power relation has been observed by a number of investigators. Liu [8] has pointed out that localized necking at a crack tip may lead to an exponent larger than 2. McClintock [11] has derived the fourth power relation from a model that includes a length factor of the microstructure of a material. Rice [12] derived the fourth power relation from a rigid plastic strip model, which assumes that plastic deformation is limited to a strip of materials ahead of a crack tip. A realistic physical explanation for Rice's rigid-plastic strip model is the necking model proposed by Liu [8].

More recently Lehr and Liu [13] have proposed a simple phenomenological model of fatigue crack propagation. It assumes that crack propagation is caused by cumulative damage due to strain cycling of the material at a crack tip. With Miner's linear cumulative damage law and Manson and Coffin's strain cycling fatigue law, a fatigue crack propagation rate was calculated.

The model is based on the assumption that damage is caused by cyclic straining of the material. During recent years, numerous investigations have been made on fatigue damage using transmission electron microscopy to study dislocation structures [18, 19], and microscopic studies on surface and subsurface damages [20, 21]. These studies have shown that plastic strain causes high dislocation density and sub-grain structures, hence strain hardening, and that repeated plastic deformation causes fissures and microcracks in crystalline materials. Such damages to a material will be accumulated as the number of cycles of loading increases.

Recent fractographic studies [14-17] have shown striations on fracture surface. Several models for striation formation have been proposed. The 'plastic blunting process' proposed by Laird and Smith [16] associates striation formation with plastic deformation at a crack tip. If all of the length parameters, such as Burgers vector etc., associated with the deformation process are small in comparison with the size of incremental crack growth, a continuum approach, such as the model proposed by Lehr and Liu, can be used for analyzing fatigue crack propagation.

In this study, fatigue crack propagation rates in 2024-T351 aluminum alloy and 4340 fully annealed steel specimens were measured. Strain controlled fatigue properties and cyclic stress-strain curves for these two materials were measured. Deformations in front of crack tips in 2024-T351 Al specimens were measured using the moire method. The crack propagation rates in these two materials are related to their cyclic fracture ductilities.

Fatigue crack propagation and strain cycling properties of a material

It is assumed that cumulative damage by strain cycling causes a crack to propagate. The material at some distance ahead of a crack tip experiences strain cycles of increasing range as the crack propagates toward the point. If each strain cycle incurs damage to the material and if one uses Miner's cumulative damage law and Manson and Coffin's strain cycle fatigue law, an expression for fatigue crack propagation rate can be derived.

The strain field along the crack line and ahead of a crack tip can be written as

$$\epsilon/\epsilon_Y = (r/r_p)^{\beta} \tag{1}$$

where ϵ_Y is the yield strain of the material; r the distance from the crack tip; and r_p the plastic zone size. We shall discuss the significance of ϵ_Y and r_p in more detail later. It can be shown that r_p is proportional to K^2 if the applied stress is low compared with σ_Y. [8]. Therefore Equation (1) gives a relation between the strain field and the applied stress. For higher applied stresses, β may vary.

Let us assume that the cyclic life for strain controlled fatigue, N_f, is given by

$$N_f = (\Delta\epsilon/M)^{1/z} \tag{2}$$

where $\Delta\epsilon$ is total strain range, and M and z are constants. Equation (2) is similar to Manson-Coffin's strain controlled fatigue law, [22, 23, 24], except that $\Delta\epsilon$ in Equation (2) is total strain range rather than plastic strain range as proposed by Manson and Coffin. Since our interest is in the very high strain region and elastic strain is usually negligible, Equation (2) is equivalent to Manson-Coffin's strain controlled fatigue law.

For the material at a distance r_i away from the crack tip, the strain range is

$$\Delta\epsilon_i = \epsilon_Y\,(r_i/r_p)^{\beta} \tag{3}$$

For this strain range, the cyclic life is

$$N_{fi} = (\epsilon_Y/M)^{1/z}(r_i/r_p)^{\beta/z} \tag{4}$$

Since the material at r_i experiences the strain cycle only once, the cycle ratio is

$$\bar{N}_i = \frac{1}{N_{fi}} \tag{5}$$

According to Miner's cumulative damage law [25] failure occurs when

$$\sum_{i=1}^{t} \bar{N}_i = 1 \tag{6}$$

where t is the total number of cycles experienced by the material at a fixed point after it enters r_p. When the applied stress is very low, r_p is small in comparison with other dimensions of the specimen. Therefore the stress intensity factor is essentially constant after the material at a fixed point enters r_p, and it is reasonable to expect that the crack increment per cycle, Δr, is essentially constant during this period of time. Thus

$$t = \frac{r_p}{\Delta r} \tag{7}$$

Multiplying Equation (6) by Δr_i, one obtains,

$$\frac{da}{dN} = \sum_{i=1}^{t} \bar{N}_i \Delta r_i = \left(\frac{M}{\epsilon_Y}\right)^{1/z} r_p \sum_{i=1}^{t} \left(\frac{r_i}{r_p}\right)^{-\beta/z} \frac{\Delta r_i}{r_p} \tag{8}$$

For a given set of values of β, z and r_p, the sum is a constant. If the increment is small and $\bar{N}_i$ is a smooth function of r, Equation (8) can be approximated by

$$\frac{da}{dN} = \left(\frac{M}{\epsilon_Y}\right)^{1/z} r_p \int_0^{r_p} \left(\frac{r}{r_p}\right)^{-\beta/z} d\left(\frac{r}{r_p}\right) \tag{9}$$

After integration, it becomes

$$\frac{da}{dN} = \left(\frac{M}{\epsilon_Y}\right)^{1/z} \frac{r_p}{1-\beta/z} \tag{10}$$

provided $(1-\beta/z) > 0$. If $(1-\beta/z) \leq 0$, the integral does not converge. In this case the summation expression, Equation (8), can be used but the sum does not converge to a given value. As it was pointed out da/dN is Δr_i, therefore, the value of Δr_i for the sum has to be adjusted so that Equation (8) is satisfied. In this case for a given set of values of M, ϵ_Y, β, z and r_p, the sum is a constant. Both the integral and the sum are very sensitive to the quantity $(1-\beta/z)$. Both β and z have values very close to each other, and neither β nor z can be determined accurately. Thus we shall write

$$\frac{da}{dN} = \gamma\, r_p \left(\frac{M}{\epsilon_Y}\right)^{1/z} \tag{11}$$

where γ is a proportional constant. The expression indicates that crack propagation rate is proportional to r_p and the quantity $(M/\epsilon_Y)^{1/z}$. If the relationship between r_p and stress intensity factor range, ΔK, is known, da/dN can be expressed in terms of ΔK.

Examining the model closely, one concludes that da/dN is proportional to r_p, because of the application of the continuum model and the strain field given by Equation (1); and da/dN is proportional to $(M/\epsilon_Y)^{1/z}$ because of the choice of Manson-Coffin's law for fatigue damage and Miner's law for damage accumulation.

The proposed model assumes a strain field as given by Equation (3). The strain range is given in terms of the normalized coordinate (r/r_p). As a crack propagates, the material within an increment Δr, should experience the same stress and strain histories, if $\Delta r/r_p$ has the same value. Consequently a continuum model should predict that da/dN is proportional to r_p, regardless of the choices of fatigue damage law and the law for damage accumulation.

The above result is contingent upon the assumption that the length parameters of deformation process and crack growth process are small in comparison with incremental crack length, so that a continuum model is applicable. McClintock [11] has shown that if a microstructural length, which is pertinent to crack propagation, is comparable to the size of incremental crack growth, da/dN is proportional to ΔK^4.

Equation (11) indicates that da/dN is proportional to $(M/\epsilon_Y)^{1/z}$. The quantity M is the strain range corresponding to a cyclic life $N_f = 1$. It is a measure of the capability of a material to sustain cyclic deformation. If one accepts the crack propagation model based on cumulative damage caused by cyclic straining, it is reasonable to expect that da/dN is related to the quantity (M/ϵ_Y). The quantity M is normalized by ϵ_Y, because of the strain field given by Equation (1). The specific relation between da/dN and (M/ϵ_Y) is derived from Miner's cumulative damage law. For example, if one wishes to emphasize the damage incurred by cycles of high strain range, i.e. the strain cycles when the point is very close to the crack tip, and assumes,

$$\sum_{i=1}^{t} (\bar{N}_i)^2 = 1 \tag{12}$$

as the condition of failure, one concludes that da/dN is proportional to $(M/\epsilon_Y)^{2/z}$. Therefore the specific relation between da/dN and (M/ϵ_Y) depends upon the choice of a specific cumulative damage law.

It can be concluded that da/dN is proportional to r_p, because of the application of the continuum model and the strain field given by Equation (3); and da/dN is proportional to $(M/\epsilon_Y)^{1/z}$ because of the application of Manson-Coffin's law for fatigue damage and Miner's law for damage accumulation.

Let us examine the significance of ϵ_Y and r_p in Equation (3) which can be written in the form

$$\Delta\epsilon = \frac{\epsilon_Y}{(r_p)^\beta} (r)^\beta \tag{13}$$

The quantity $\epsilon_Y/(r_p)^\beta$ determines the intensity of a strain field, and $(r)^\beta$ determines the distribution of the strain field. We have defined ϵ_Y and r_p as yield strain and the size of plastic zone. But one can choose any arbitrary high strain ϵ_Y' and corresponding to ϵ_Y' there is a highly strained region r_p'. The significant fact is that the quantity, $\epsilon_Y'/(r_p')^\beta$ or $\epsilon_Y/(r_p)^\beta$ prescribes the strain intensity near a crack tip.

Experimental results

Fatigue crack propagation rate, and static and cyclic tensile properties were measured on 2024-T351 aluminum alloy and 4340 fully annealed steel. Strains at crack tips in 2024-T351 Al specimens were measured to provide the relationship between r_p and ΔK.

Centrally cracked specimens were used for the propagation study. The specimen width was 4 in. The thicknesses were ¼ in for 2024-T351 Al and ⅛ in for 4340 steel. The crack propagation data for these two

materials are shown in Figs. 1 and 2. The ratio of $\sigma_{min}/\sigma_{max}$ was 0·1 for all tests. The crack propagation data for 2024-T351 aluminum alloy show three regions of crack propagation, in the region of high stress intensity factor range, ΔK, the slope of the line is 4, in the intermediate ΔK region the slope is 2·6, and in the low ΔK region the slope is close to 5. ΔK is defined as $\Delta\sigma\sqrt{(a)}$ for a centrally cracked infinite plate, and Ishida's correction for finite plate was used. The applied stresses are indicated in the figure.

It is unlikely that one could correlate the data in all three regions using a simple model as proposed in this study. Therefore it is important to analyze the reasons for the differences between these three regions. In region I, the slope is 5 and the propagation rate is 4×10^{-6} in per cycle or less. When ΔK was reduced to 1·25 $KSI\sqrt{(IN)}$, after half a million cycles, the crack propagated less than 0·0005 in, which gives a crack propagation rate less than 10^{-9} in per cycle. The Burgers vector and the atomic size of aluminum are nearly 10^{-8} in which is still two orders of magnitude smaller than 10^{-6} in. However the distance between dislocation sources, average distance travelled by dislocations, size of dislocation network etc. could be important. Therefore 10^{-6} in may be comparable to a structural size which is pertinent to crack growth. Hence in region I, the proposed continuum model is not applicable.

In the high ΔK region, i.e. region III, measured propagation rate is proportional to ΔK^4. Liu [8] has pointed out that as a crack propagates, stress intensity factor and plastic zone size increase. When the plastic zone size becomes comparable to the thickness of a plate, there is a fracture transition from the normal mode to a shear mode. After transition r_p increases rapidly, and deformation becomes highly localized within a narrow strip because of necking. The size of the strip is restricted by the plate thickness. In this case, Rice's rigid plastic strip model is applicable and da/dN becomes proportional to ΔK^4. Therefore in region III, da/dN is strongly influenced by a necking process and the plate thickness. The proposed model does not take such effects into consideration. Furthermore, when a specimen reaches region III, its life expectancy is short, consequently there is less practical interest.

In the intermediate ΔK region, i.e. region II, da/dN is proportional to $\Delta K^{2\cdot6}$. In this region a simple strain field as given by Equation (1) is applicable as was shown by strain measurements. The region occurs prior to the fracture mode transition so that crack propagation is not complicated by a necking process. Consequently, we shall concentrate our analysis on region II.

Figure 2 shows the data for 4340 fully annealed steel both in region II and III. da/dN is proportional to $\Delta K^{2\cdot6}$ in region II, and it is proportional to ΔK^4 in region III. Crack propagation transitions from region II to region III take place at 13 $KSI\sqrt{(IN)}$ and 25 $KSI\sqrt{(IN)}$ for 2024-

T351 Al and 4340 steel specimens respectively. The fracture mode transitions from normal to shear are completed at 14 $KSI\sqrt{(IN)}$ and 30 $KSI\sqrt{(IN)}$ for these two materials, but they start much earlier.

In order to correlate experimental data with Equation (11), the relationship between ΔK and r_p is required. The moire method [26, 27] was used to measure the strains ahead of crack tips in 2024-T351 aluminum specimens. A two thousand line per inch grille was printed on the specimen surface using 'photo resist'. The lines were parallel to the crack. After printing, the crack was propagated by cyclic loading. When the crack reached a predetermined length, a moire fringe picture was taken at the maximum stress level using a reference grille of the same line density. Strain is simply calculated from $\epsilon = p/d$, where p is the pitch of the grille, and d is fringe spacing. The results are shown in Fig. 3. The value of ΔK for each line is indicated. Two sets of measurements were made on two different specimens for ΔK at 18 $KSI\sqrt{(IN)}$. These two sets of measurements are close to each other. The slopes of the lines in a log-log plot vary from −0·50 to −0·54. The average is −0·52.

The size of r_p was determined by the intersection of these lines with a strain of 0·0134 in/in which corresponds with the cyclic yield strength of the material. Notice that the curve for $\Delta K = 18$ $KSI\sqrt{(IN)}$ tends to level off and deviate from the straight line. However r_p was obtained by extrapolating the straight line rather than by following the actual curve. As discussed earlier, r_p can be viewed as a fictitious quantity, which characterizes the strain amplitude within the region of r_p. Therefore, the intersection with the extrapolated straight line should give a better result.

The values of r_p are plotted against ΔK in Fig. 4. In the lower region r_p is proportional to ΔK^2. In the upper region r_p is proportional to ΔK^3. The data have a transition point at ΔK approximately equal to 17 $KSI\sqrt{(IN)}$. The results in Fig. 4 give the following empirical relation

$$r_p = 1{\cdot}30\left(\frac{\Delta K}{\sigma_{Y(c)}}\right)^2 \tag{14}$$

where $\sigma_{Y(c)}$ is the cyclic yield strength of the material which is 134×10^3 lb/in^2.

To determine r_p, either the cyclic yield strain $\epsilon_{Y(c)}$ or the static yield strain $\epsilon_{Y(s)}$ can be used. The size of the plastically deformed region is undoubtedly influenced to a great extent by the static yield strain. On the other hand, the proposed model of crack propagation is based on the cyclic plastic deformation at a crack tip. Therefore $\epsilon_{Y(c)}$ was used to determine r_p.

In Fig. 5, the strain controlled fatigue data on 2024-T351 aluminum alloy and 4340 fully annealed steel are plotted. The values of M are 0·30

and 0·47 for 2024-T351 aluminum alloy and 4340 fully annealed steel respectively. Additional data in the high strain region are needed to determine M more accurately. The slopes of both lines are close to −0·5.

The cyclic stress strain curves for these two materials are shown in Fig. 6. The cyclic stress strain curve was determined by the tips of the stable hysteresis loops for cyclic tests at several completely reversed strain ranges [28]. Each cyclic test gives one point on the diagram. The total stress range and total strain range are plotted. The cyclic yield strength and strain are determined by the intersection of the elastic line with the line in the plastic region. The values of $\sigma_{Y(c)}$ are 134×10^3 lb/in^2 and 160×10^3 lb/in^2 for 2024-T351 aluminum and 4340 steel respectively. The values of $\epsilon_{Y(c)}$ are 0·0134 and 0·0053.

With $z = -0{\cdot}5$, Equations (11) and (14) lead to

$$\frac{da}{dN} = \bar{\gamma}\left[\frac{\Delta K}{\sigma_{Y(c)}}\right]^2\left[\frac{\epsilon_{Y(c)}}{M}\right]^2 \tag{15}$$

If one assumes that Equation (14) is applicable to both the aluminum alloy and the steel, one can use Equation (15) to calculate crack propagation rate for these two materials. The solid lines in Fig. 7, are crack propagation data in region II for both 2024-T351 aluminum and 4340 steel. The dashed lines are calculated from Equation (15) with $\bar{\gamma} = 3{\cdot}6$. The empirical equation for the data, i.e. solid lines, is

$$\frac{da}{dN} = 11\left[\frac{\Delta K}{\sigma_{Y(c)}}\right]^{2{\cdot}6}\left[\frac{\epsilon_{Y(c)}}{M}\right]^{1{\cdot}9} \tag{16}$$

The correlation is surprisingly good. The maximum deviation between measured and calculated propagation rates is approximately 50%. The slopes of the empirical lines are 2·6 instead of 2. The difference could be caused by thickness effect and/or by fracture of brittle particles. Kershaw and Liu [17] have found that striation spacing in a 7075-T6 aluminum sheet was proportional to $\Delta K^{1{\cdot}8}$, but the surface crack propagation rate was proportional to $\Delta K^{2{\cdot}8}$. It was found that the fracture of brittle particles causes differences between the surface crack propagation rate and striation spacing. Bates and Clark [14] found that striation spacing as well as overall crack propagation rate for a number of materials were proportional to ΔK^2. They used very thick specimens, so that the propagation rate was not affected by necking. These two factors may account for the difference between the experimental and the theoretical exponents on the quantity $(\Delta K/\sigma_{Y(c)})$.

The experimental results indicate strongly that the fatigue crack propagation resistence of a material is related to its cyclic fracture ductility, i.e. the quantity $(M/\epsilon_{Y(c)})$, which reflects the capability of a material to sustain cyclic deformation.

Summary and Conclusions

1. A mechanical model of fatigue crack propagation is proposed. It is hypothesized that fatigue crack propagation is caused by damage accumulation due to strain cycling of the material at a crack tip.

2. The fatigue crack propagation resistance of a material is related to its cyclic fracture ductility, $(M/\epsilon_{Y(c)})$.

3. Correlation of the proposed theory with experimental data for 2024-T351 aluminum alloy and 4340 fully annealed steel was surprisingly good.

4. Strain at a crack tip is porportional to ΔK^2 and $r^{-1/2}$.

Acknowledgments

The investigation was conducted at the Metallurgical Research Laboratories at Syracuse University. The support by NASA, Grant NGR 33-022-032, made the investigation possible. The authors are indebted to U.S. Steel Corporation for their supply of the 4340 steel, to Messers. John J. McKeon and Chellis Chave for their assistance in laboratory testing and to Mmes. Helen Turner and Barbara Howden for the preparation of the manuscript.

References

1. FROST, N. D. & DUGDALE, D. S. 'The propagation of fatigue cracks in sheet specimens', *Journal of Mechanics and Physics of Solids*, vol. 6, no. 2, 1958.
2. McEVILY, Jr. A. J. & ILLG, W. 'The rate of fatigue-crack propagation in two aluminum alloys', *Natl. Adv. Comm. Aero.*, TN 4394, September 1958.
3. LIU, H. W. 'Crack propagation in thin metal sheet under repeated loading', *Journal of Basic Engineering*, Series D, Trans. ASME, vol. 83, pp. 23-31, 1961.
4. PARIS, P. C., GOMEZ, M. P. & ANDERSON, W. E. 'A rational analytic theory of fatigue', *The Trend in Engineering*, University of Washington, 1961.
5. LIU, H. W. 'Fatigue crack propagation and applied stress range', *ASME Trans. J. Basic Eng.*, March 1963.
6. PARIS, P. & ERDOGAN, F. 'A critical analysis of crack propagation laws', *Journal of Basic Engineering, Trans. ASME*, Series D, 1963.
7. WEISS, V. & SESSLER, J. 'Strain controlled fatigue in pressure vessel materials', Winter Annual Meeting of ASME, November 1963.
8. LIU, H. W. 'Fatigue crack propagation and the stresses and strains in the vicinity of a crack', Appl. Materials Research, October, 1964.
9. PARIS, P. 'Fracture mechanics approach to fatigue', Tenth Sagamore Army Materials Research Conference, 1963.
10. SCHIJVE, S. 'Significance of fatigue cracks in micro-range and macro-range', *Fatigue crack Propagation ASTM STP 415*, Am. Soc. for Testing and Materials, 1967.
11. McCLINTOCK, F. A. 'On the plasticity of the growth of fatigue cracks', *Fracture of Solids*, Met. Soc. AIME Conf. 20, Interscience, New York, 1963.
12. RICE, J. 'Plastic yielding at a crack tip', The First International Conference on Fracture, Sendai, Japan, 1965.
13. LEHR, K. R. & LIU, H. W. 'Fatigue crack propagation and strain cycling properties', Syracuse University Research Institute, Technical Report, July 1968.

14. BATES, R. C. & CLARK, Jr. W. G. 'Fractography and fracture mechanics', Scientific Paper 68-1D7-RDAFC-P1, Westinghouse Research Laboratories, Pittsburgh, Pennsylvania.
15. FORSYTH, P. J. E. & RYDER, P. A. 'Fatigue fracture', *Aircraft Engineering*, vol. 32, no. 374, p. 96, 1960.
16. LAIRD, C. & SMITH, G. C. 'Crack propagation in high stress fatigue', *Philosophical Magazine*, vol. 7, p. 847, 1962.
17. KERSHAW, J. & LIU, H. W. 'Electron fractography and fatigue crack propagation in 7075-T6 aluminum sheet', presented at the Symposium on Electron Fractography, ASTM Annual Meeting, San Francisco, June, 1968.
18. GROSSKREUTZ, J. C. & WALDOW, P. 'Substructure and fatigue fracture in aluminum', *Acta Met.*, vol. 11, no. 7, 1963.
19. FELTNER, C. E. 'Dislocation arrangements in aluminum deformed by repeated tensile stresses', *Acta Met.*, vol. 11, pp. 817-828, 1963.
20. HOLDEN, J. 'The formation of sub-grain structure by alternating plastic strain', *Phil. Mag.*, vol. 6, pp. 547-558, 1961.
21. WOOD, W. A., COUSLAND, S. M. & SARGANT, K. R. 'Systematic microstructural changes peculiar to fatigue deformation', *Acta Met.*, vol. 11, no. 7, 1963.
22. MANSON, S. S. 'Fatigue: a complex subject — some simple approximations', William M. Murray Lecture — 1964, *Experimental Mechanics*, pp. 193-226, July 1965.
23. MANSON, S.S. & HIRSCHBERG, M. H. 'Fatigue behavior of materials under strain cycling in the low and intermediate cycle range', *Fatigue — An Interdisciplinary Approach*, ed. by J. J. Burke, N. L. Reed, and V. Weiss, Syracuse University Press, pp. 133-173, 1964.
24. COFFIN, Jr. L. F. 'A study of effects of cyclic thermal stresses on a ductile metal', *Trans. ASME*, vol. 76, no. 6, pp. 931-949, August, 1954.
25. MINER, M. A. 'Cumulative damage in fatigue', *J. Appl. Mech.*, vol. 12, no. 3, pp. A159-A164, September, 1945.
26. DANTU, P. 'Investigating deformation by means of gratings', The Central Technical Information Service, C. E. Trans. No. 3089.
27. SCIAMMARELLA, C. A. & DURELLI, A. J. 'Moire fringes as a means of analyzing stress', *J. of Eng. Mechanics Div., Proc. of ASCE*, Feb. 1961, E 1, p. 55.
28. LANDGRAF, W., MORROW, JODEAN & ENDO, T. 'Determination of the cyclic stress-strain curve', Presented at ASTM 70th Annual Meeting, Boston, June, 1967.

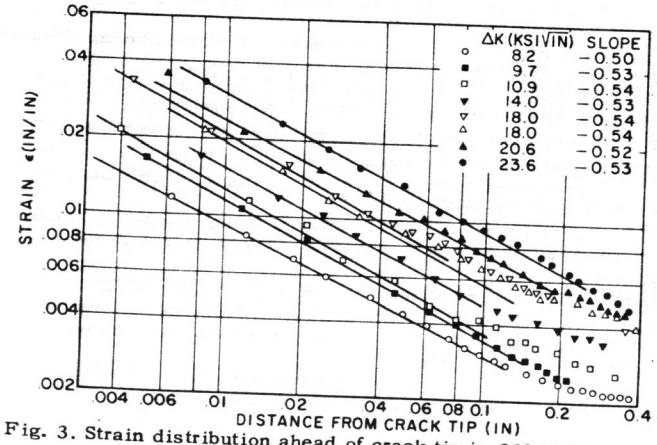

Fig. 3. Strain distribution ahead of crack tip in 2024-T351 Al specimen.

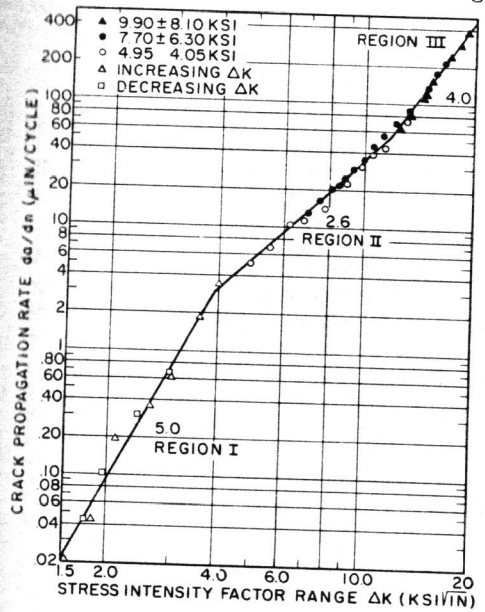

Fig. 1. Crack propagation rate vs. stress intensity factor range for 2024-T351 Al

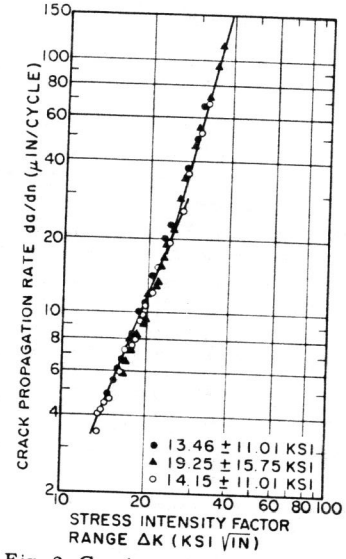

Fig. 2. Crack propagation rate vs. stress intensity factor range for 4340 fully annealed steel.

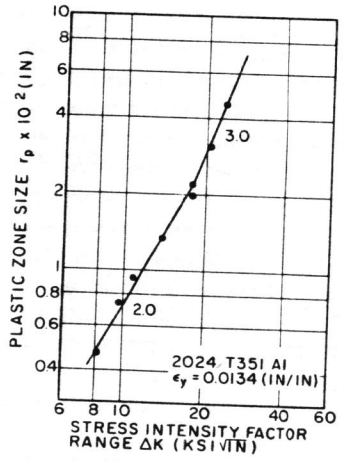

Fig. 4. Plastic zone vs. stress intensity factor range for 2024-T351 Al.

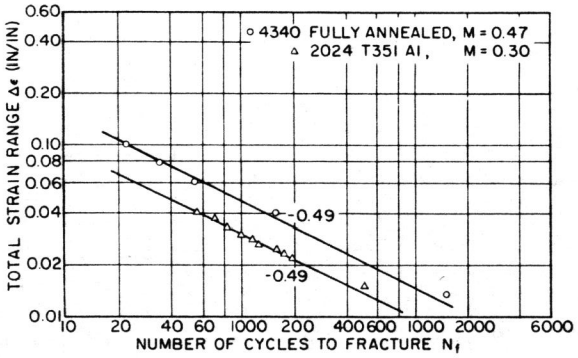

Fig. 5. Fatigue behavior of 2024-T351 Al and 4340 fully annealed steel at high strain ranges.

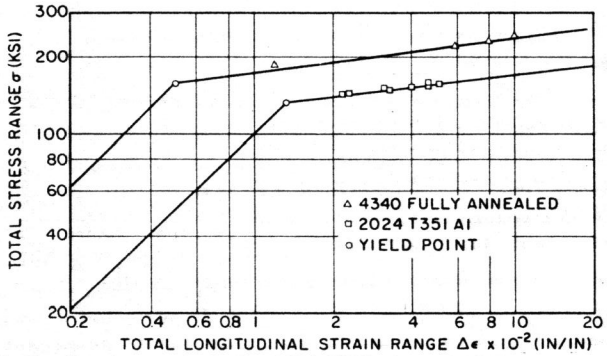

Fig. 6. Cyclic stress-strain for 2024-T351 Al and 4340 fully annealed steel specimen.

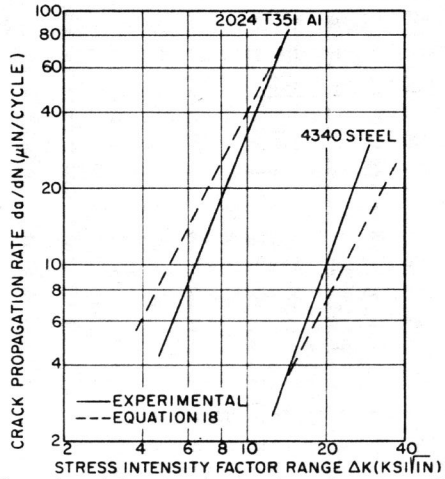

Fig. 7. Experimental and calculated crack propagation rates vs. stress intensity factor range.